IET Renewable Power Generation

*Research Article*

IET Journals
The Institution of Engineering and Technology

# Dual-function PV-ECS integrated to 3P4W distribution grid using 3M-PLL control for active power transfer and power quality improvement

ISSN 1752-1416
Received on 13th August 2016
Revised 18th December 2017
Accepted on 26th February 2018
E-First on 8th May 2018
doi: 10.1049/iet-rpg.2016.0723
www.ietdl.org

*Rahul Kumar Agarwal[1], Ikhlaq Hussain[1] ✉, Bhim Singh[1]*
[1]*Department of Electrical Engineering, IIT Delhi, New Delhi 110016, India*
✉ *E-mail: ikhlaqb@gmail.com*

**Abstract:** This study proposes a single-stage solar photovoltaic energy conversion system (PV-ECS) integrated to a three-phase four-wire (3P4W) distribution grid with dual-function capabilities, i.e. active power transfer and power quality (PQ) enhancement at the point of interaction (PoI). The PV-ECS system comprises of a solar photovoltaic array and a voltage source inverter (VSI), supplying active power (during daytime) to the distribution grid and connected single-phase and three-phase loads. Apart from transfer of power, the system also improves the PQ at the PoI by compensating reactive power and neutral current, attenuating harmonics, correcting power factor and balancing grid currents. During night, the VSI acts as a shunt active power filter mitigating PQ issues, thereby increasing the device utilisation factor. A three-phase magnitude-phase locked loop (3M-PLL) method is utilised to extract and estimate fundamental term of load currents and an incremental conductance algorithm is applied for maximum power point tracking. To demonstrate its effectiveness, the system is modelled and its performance is simulated on MATLAB and experiments are performed on a developed prototype in the laboratory.

## 1 Introduction

With the objective of achieving urban sustainability, the installation of solar photovoltaic-energy conversion system (PV-ECS) on rooftops of commercial and industrial buildings is proving as a prime strategy [1]. The Indian government has unveiled solar programs for installing grid-integrated PV-ECS of about 40 GW capacity by the end of the year 2022 [2]. This is expected to result in the decrease in the prices of the solar photovoltaic (PV) system and to attain grid parity.

Instead of using single-phase [3, 4] and three-phase three-wire [5] grid-integrated solar PV systems, it is desirable to install three-phase four-wire (3P4W) grid-integrated PV-ECS. The main benefit of a 3P4W distribution network over a three-phase three-wire and single-phase distribution networks is that it can supply power to both single-phase and the three-phase connected loads at the same time. Therefore, today for construction of sustainable buildings, a 3P4W distribution grid-connected rooftop solar PV-ECS has caught the centre of attention. Moreover, a PV-ECS system with enhanced capabilities at the users end is preferred over conventional solar PV systems, which can only fulfil active power need of the grid and loads. The PV-ECS system supplies active power and aids in power quality enhancement at the point of interaction (PoI). This reduces the burden on the centralised active power filters, which are installed at various substations. The functionalities of a shunt active power filter (SAPF) are reported in the literature [6] using various control algorithms such as artificial neural network (ANN) [7], combined least mean square–least mean fourth [8], adaptive neuro fuzzy inference system [9], robust DC link voltage control, sliding mode control [10], frequency-adaptive fractional-order repetitive [11] and linear quadratic Gaussian control [12].

Another important issue with PV-ECS is the varying environmental conditions. As the solar irradiance incident on the earth changes from point to point and time to time, therefore, it is vital that solar PV array is made to operate at its maximum power point (MPP) thereby extracting maximum power at every solar irradiation level. For extraction of maximum power from PV-ECS, MPP tracking (MPPT) techniques are used such as linearisation controller presented by Espinoza-Trejo *et al.* [13], which has a capability to track even with fast changes in solar irradiation levels. Paz and Ordonez [14] have discussed a switching ripple identification technique for reducing the ripples and eliminating the oscillations during the steady-state operation. Other MPPT techniques like improved incremental conductance (InC) [15, 16], fast-converging technique [17], Grey-wolf optimisation technique [18], adaptive fuzzy [19] and ANN [20] are also reported in the literature. Some other topologies have also been reported in the literature such as cross-source energy harvesting circuit [21], sub-module integrated converters [22] and single-ended primary-inductor converter using adaptive voltage-sensor-based control [23].

The use of non-linear loads at the PoI injects various harmonics on the grid side currents, which have adverse effects on the operation of control and protection devices connected to the system. Therefore, to eliminate the noise and distortions, a three-phase magnitude-phase locked loop (3M-PLL) technique is used, which provides frequency estimation, peak detection, filtering, harmonics extraction, disturbance detection and so on [24]. Particularly, the 3M-PLL technique is used as an anti-aliasing filter for three-phase non-linear signals, generating output with zero bias and zero phase shift in the signals. In comparison with the conventional PLL techniques reported in the literature [25], it differs in a way that the proposed 3M-PLL technique uses a linear feedback loop and its robust nature and simple structure make it more suitable for a three-phase system.

The major contributions proposed in this paper include:

- Active power transfer to 3P4W distribution grid and connected single-phase and three-phase loads with power quality enhancement.
- Application of 3M-PLL technique based control algorithm for filtering the non-linear load currents.
- Increased utilisation factor of voltage source inverter (VSI) during night when the solar power is unavailable.
- Extraction of maximum power from the PV-ECS using MPPT method based on InC algorithm, which is adaptable to variation in solar irradiance levels.

For demonstrating the proficiency of the proposed system, component design and system modelling of 3P4W grid-integrated

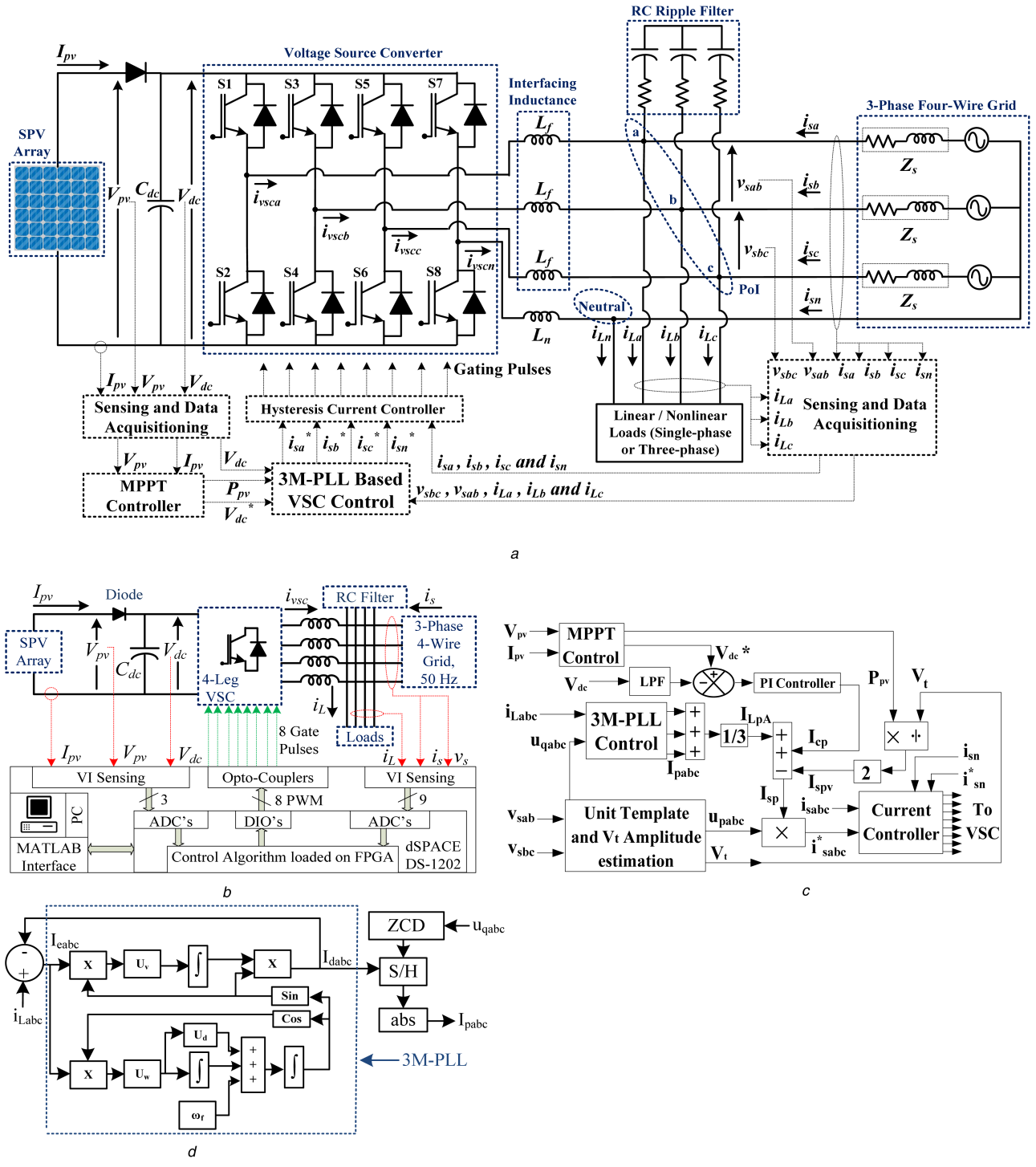


**Fig. 1** *System configuration and control scheme*

***(a)*** Structure diagram of 3P4W grid-connected PV-ECS, ***(b)*** Block diagram of experimental prototype for 3P4W grid-integrated PV-ECS, ***(c)*** Control scheme for 3P4W grid-tied PV-ECS, ***(d)*** Block diagram of the 3M-PLL technique

PV-ECS using single-stage VSI controlled by InC-MPPT and 3M-PLL algorithm are carried out and simulations are performed in MATLAB. A prototype of the proposed system is developed in the laboratory for evaluating the varying responses of it.

## 2 Structure and control strategy of grid-connected PV-ECS

The schematics and block diagram of an experimental prototype of 3P4W grid-integrated PV-ECS are shown in Figs. 1*a* and *b*. The system utilises a solar PV array, an insulated gate bipolar transistor based four-leg VSI with a DC link capacitor ($C_{dc}$), an interfacing inductance ($L_f$), a ripple filter, a 3P4W grid having a source impedance ($Z_s$) and connected single-phase or three-phase non-linear or linear loads. The ripple filters are utilised to attenuate the high switching noise produced from the operation of the VSI. Moreover, the function of interfacing inductance ($L_f$) is to attenuate the ripples, which are present in the currents produced by the VSI. The detailed analyses for the design of aforementioned components are reported in the literature [6, 26, 27].

The control strategy for a proposed single-stage solar PV-ECS tied to a 3P4W distribution grid is shown in Fig. 1*c*. The use of a single-stage topology reduces the number of components in the PV-ECS thereby reducing losses and increases the efficiency. The control strategy comprises of two main constituents, which are: (i) InC-based MPPT control and (ii) 3M-PLL-based switching control of VSI.

**Table 1** Simulation parameters

| | | | |
|---|---|---|---|
| PV array power $P_{pv}$ | 32.4 kW | PV voltage, $V_{pv}$ and current, $I_{pv}$ | 710 V and 45.6 A |
| interfacing inductor, $L_f$ | 2.5 mH | DC bus voltage, $V_{dc}$ | 710 V |
| grid voltage, $v_{ab}$ | 415 V (rms) | sampling time, $T_s$ | 1 μs |
| DC PI controller, $K_{pd}$ and $K_{id}$ | 1.35 and 1 | ripple filter, $R_f$ and $C_f$ | 5 Ω and 10 μF |
| non-linear load | three one-phase DBR feeding $R$ = 5 Ω and $L$ = 100 mH load | constants, $u_v$, $u_d$ and $u_w$ | 100, 0.005 and 200 |

### 2.1 InC-based MPPT control

A substantial research work has been done on MPPT control so far and various techniques have been described in the literature [13–20]. Of several algorithms, InC approach is utilised here to achieve MPPT. The main function of this block is to input sensed PV voltage ($V_{pv} = V_{dc}$) and current ($I_{pv}$) to compute PV power ($P_{pv}$) along with the estimation of reference DC link voltage ($V_{dc}$*). It is generated as an output for extracting the maximum power.

### 2.2 3M-PLL-based switching control of VSI

This section describes the approach utilised for the estimation and extraction of fundamental components of load currents, loss components, feed-forward component, reference grid currents and generating the gate pulses for switching of three-phase VSI.

*2.2.1 Calculation of unit templates:* From sensed PoI line voltages ($v_{sab}$, $v_{sbc}$), the phase voltages at the PoI are obtained from equation reported in [27] as

$$v_{sa} = \frac{2v_{sab} + v_{sbc}}{3}; \quad v_{sb} = \frac{-v_{sab} + v_{sbc}}{3}; \quad v_{sc} = \frac{-v_{sab} - 2v_{sbc}}{3} \tag{1}$$

The peak amplitude of terminal voltage ($V_t$) is evaluated as

$$V_t = \sqrt{\frac{2}{3}(v_{sa}^2 + v_{sb}^2 + v_{sc}^2)} \tag{2}$$

The in-phase unit templates and quadrature unit templates are estimated as

$$u_{pa} = \frac{v_{sa}}{V_t}; \quad u_{pb} = \frac{v_{sb}}{V_t}; \quad u_{pc} = \frac{v_{sc}}{V_t} \tag{3}$$

$$u_{qa} = -\frac{u_{pb}}{\sqrt{3}} + \frac{u_{pc}}{\sqrt{3}}; \quad u_{qb} = \frac{\sqrt{3}u_{pa}}{2} + \frac{(u_{pb} - u_{pc})}{2\sqrt{3}}; \quad u_{qc} = -\frac{\sqrt{3}u_{pa}}{2} + \frac{(u_{pb} - u_{pc})}{2\sqrt{3}} \tag{4}$$

*2.2.2 Calculation of loss component and PV feed-forward term:* The DC link voltage error ($V_{de}$) is evaluated as difference between $V_{dc}$* and sensed DC voltage ($V_{dc}$) as

$$V_{de}(n) = V_{dc}^*(n) - V_{dc}(n) \tag{5}$$

where $V_{dc}$*($n$) is switched as per the mode of operation. During daytime operation, $V_{dc}$* is achieved from the MPPT block and during night-time operation as a SAPF, $V_{dc}$* is set as $V_{dc\_DST}$, which is calculated as

$$V_{dc\_DST} = 2\sqrt{2}V_{sab}(n)/\sqrt{3}m \tag{6}$$

where $m$ is the inverter amplitude modulation index and is taken here $m$ = 1.

The error is fed to proportional–integral (PI) controller to generate the active loss component '$I_{cp}$', which is evaluated as

$$I_{cp}(n+1) = I_{cp}(n) + K_{pd}(V_{de}(n+1) - V_{de}(n)) + K_{id}V_{de}(n+1) \tag{7}$$

where $K_{pd}$ and $K_{id}$ are proportional and integral gain constants utilised in the PI controller.

The feed-forward component from solar PV array power is estimated as

$$I_{spv}(n) = \frac{2P_{pv}(n)}{(3V_t)} \tag{8}$$

where $P_{pv}$ is power extracted from PV array.

*2.2.3 Evaluation of fundamental component of load currents:* The block diagram of 3M-PLL technique for extracting the fundamental components of load current is shown in Fig. 1*d*. The unit templates ($u_{qabc}$) are subjected to zero crossing detection (ZCD) block and 3M-PLL block inputs load currents ($i_{Labc}$) to generate outputs ($I_{dabc}$). The outputs of ZCD block and $I_{dabc}$ are then fed to the sample and hold logic, which samples and holds the value of load current generated by the 3M-PLL block at every ZCD of the unit vector and then it passes the absolute value, which is the fundamental component ($i_{pabc}$) of load currents, where $u_v$, $u_w$ and $u_d$ are three different parameters, which control the operation of the 3M-PLL technique. These constants ($u_v$, $u_w$ and $u_d$) affect the system performance wherein, $u_v$ controls the settling time and magnitude response of the system and $u_w$ and $u_d$ make the response slow and oscillatory. The values chosen for $u_v$, $u_w$ and $u_d$ are considered as 100, 0.005 and 200, respectively. The detailed analysis of choosing the appropriate values of these constants is reported in the literature [24].

*2.2.4 Evaluation of reference grid currents:* The total in-phase term ($I_{sp}$) is calculated as

$$I_{sp} = I_{LpA} + I_{cp} - I_{spv} \tag{9}$$

where $I_{LpA}$ is average amplitude of in-phase load component estimated for load balancing as

$$I_{LpA} = (I_{pa} + I_{pb} + I_{pc})/3 \tag{10}$$

The reference grid currents and reference neutral current are evaluated as

$$i_{sa}^* = I_{sp} \cdot u_{pa}; \quad i_{sb}^* = I_{sp} \cdot u_{pb}; \quad i_{sc}^* = I_{sp} \cdot u_{pc}; \quad i_{sn}^* = 0 \tag{11}$$

The difference between reference grid currents ($i_{sabc}$* and $i_{sn}$*) and sensed grid currents ($i_s$ and $i_{sn}$) is subjected to a hysteresis current regulator, which generates eight gate pulses for switching of the VSI [5].

## 3 Simulation results

For validation of the proposed 3M-PLL-based control algorithm applied to 3P4W grid-integrated PV-ECS, simulations are performed on MATLAB software using SPS toolbox. The solar PV array is modelled and designed for delivering a peak power of 30 kW [26]. The system is exposed to various conditions such as supplying power to non-linear loads under unbalanced condition and performing with changing solar irradiation levels. The design data used for the circuitry and components are given in Tables 1 and 2.

**Table 2** Experimental parameters

| | | | |
|---|---|---|---|
| $P_{pv}$ | 5.35 kW | $V_{pv}I_{pv}$ | 340 V and 15.7 A |
| $L_f$ | 2.9 mH | $V_{dc}$ | 340 V |
| $v_{ab}$ | 225 V (rms) | $T_s$ | 30 µs |
| $K_{pd}$ and $K_{id}$ | 0.25 and 0.04 | $R_fC_f$ | 5 Ω 10 µF |
| non-linear load | three one-phase DBR feeding 0.8 kW load | constants, $u_v$, $u_d$ and $u_w$ | 100, 0.005 and 200 |

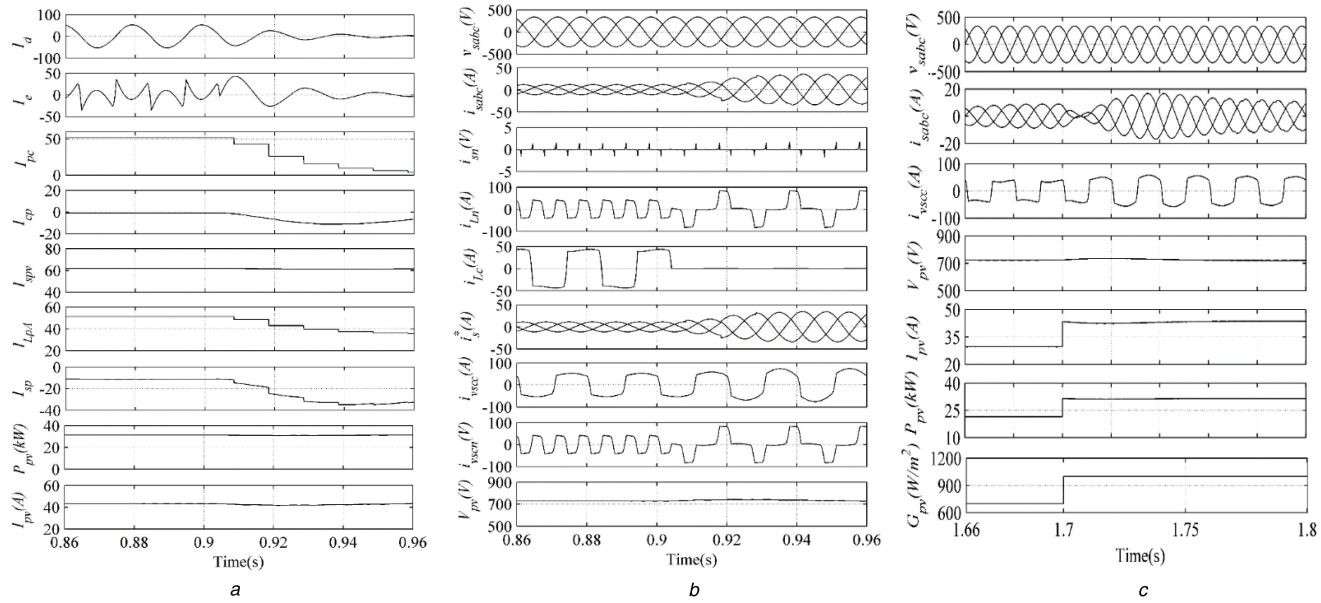


*a* *b* *c*

**Fig. 2** *Dynamic behaviour of system at*
***(a), (b)*** Unbalanced load, ***(c)*** Step increase in irradiance from 700 to 1000 W/m$^2$

**Table 3** System performance indices

| Mode | Factors | Performances indices value |
|---|---|---|
| UPF | $i_a$ (A), %THD | 10.24 A, 3.07% |
| | $i_L$ (A), %THD | 62.87 A, 31.77% |
| | $V_s$ (V), %THD | 338.9 V, 0.19% |
| | $V_{dc}$, V | 700 V |

### *3.1 Operation subject to unbalanced non-linear load*

Figs. 2*a* and *b* show system dynamic behaviour when subjected to unbalanced non-linear load. Fig. 2*a* presents the wave shapes of control internal signals ($I_{dc}$, $I_{ec}$, $I_{pc}$, $I_{cp}$, $I_{spv}$, $I_{LpA}$ and $I_{sp}$), PV power ($P_{pv}$) and PV current ($I_{pv}$). Fig. 2*b* shows the wave shapes of POI voltage ($v_{sabc}$), grid currents ($i_{sabc}$), grid neutral current ($i_{sn}$), load currents ($i_{Lc}$), load neutral current ($i_{Ln}$), reference current ($i_s$*), SPV-VSI currents ($i_{spv}$), VSI neutral current ($i_{VSIn}$) and PV voltage ($V_{pv}$). The phase '*c*' load is disconnected at 0.9 s, thus reducing it to zero. The $V_{dc}$ is maintained at a desired value for the MPPT of the PV array and the grid currents in all phases are maintained sinusoidal and balanced. The system provides neutral current compensation and maintains grid neutral current to nearly zero value. Fig. 2*a* shows the variations in the internal signals on the effect of load unbalancing. The load side total harmonic distortion (THD) is 31.77%, which is decreased to 3.07% on the grid side maintaining the value of THD within the allowable limits as stated by IEEE-519 standard [28] as presented in Table 3.

### *3.2 Operation under variable solar irradiance*

Fig. 2*c* presents the system dynamic performance when it is exposed to changing irradiance levels. The irradiance level is increased from 700 to 1000 W/m$^2$ at 1.7 s. The system, which has been operating at its MPP, shifts to a new MPP at 1000 W/m$^2$ and therefore, it increases the magnitude of SECS power ($P_{pv}$), current ($I_{pv}$), grid current ($i_{sabc}$) and VSI current ($i_{VSI}$). The grid currents ($i_{sabc}$) are sustained sinusoidal and $V_{dc}$ is maintained at a desired value for MPPT of the solar PV array. The system continues operating under unity power factor (UPF) mode.

## 4 Experimental results

A prototype of the proposed system developed in the laboratory and its block diagram is shown in Fig. 1*c*. The PV array emulator (ETS600 × 17DPVF-AMETEK make) is utilised to realise the features of an actual PV array. Three single-phase diode bridge rectifiers (DBRs) feeding RL load are utilised to demonstrate three single-phase non-linear loads. To sense the circuit voltages and currents, Hall-effect current (LA55-P) and Hall-effect voltage (LV25-P) sensors are used. The control algorithm is implemented on a digital signal processor (DSPACE-1202). The power analyser (43B, Fluke make) and a DSO (DSO0614A, Agilent make) are utilised to measure the system parameters and waveforms. The design data are provided in Tables 1 and 2.

### *4.1 System behaviour at non-linear loads*

The steady-state operation of presented system subject to non-linear loading condition is shown in Figs. 3–8. Figs. 3*a–d* show the wave shapes of PoI voltage ($v_{sbc}$) and grid currents ($i_{sabc}$) and grid neutral current ($i_{sn}$). Figs. 4*a–d* show the wave shapes of PoI phase voltages ($v_{sabc}$), and load currents ($i_{Labc}$) and load neutral current ($i_{Ln}$) with PoI voltage ($v_{sbc}$). Figs. 5*a–d* show the wave shapes of PoI phase voltages ($v_{sabc}$), and VSI currents ($i_{VSIabc}$) and VSI neutral current ($i_{VSIn}$) with PoI voltage ($v_{sbc}$). Figs. 6*a–c* show the THD of the grid currents ($i_{sabc}$), which are 3.5, 4.1 and 4.7%. Fig. 6*d* shows the THD and harmonic spectrum of the PoI voltage ($v_{sbc}$). Figs. 7*a–c* show THD of load currents ($i_{Labc}$), which are 12.9, 30.5 and 39.4%. It is observed that with so much non-linearity on the load side, the harmonics injected on the grid side is <5%, i.e. within the limits of an IEEE-519 standard [28]. Finally,

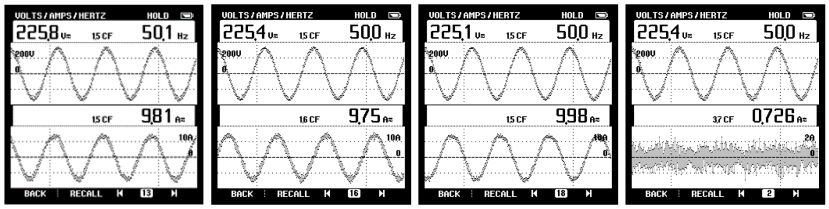


*a* *b* *c* *d*

**Fig. 3** *Steady-state responses of PV-ECS at non-linear load*
***(a)–(d)*** wave-shapes of $v_{sbc}$, $i_{sa}$, $i_{sb}$, $i_{sc}$, $i_{sn}$

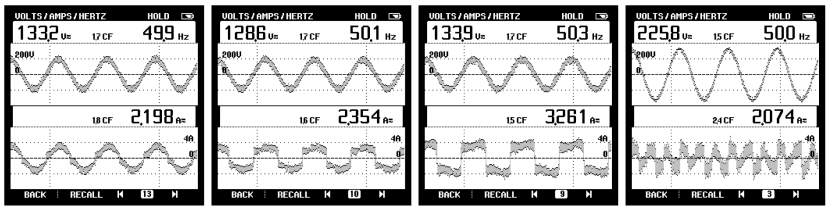


*a* *b* *c* *d*

**Fig. 4** *Steady-state responses of PV-ECS at non-linear load*
***(a)–(d)*** Wave shapes of $v_{sa}$, $i_{La}$, $v_{sb}$, $i_{Lb}$, VSI, $i_{Lc}$, $v_{sbc}$, $i_{Ln}$

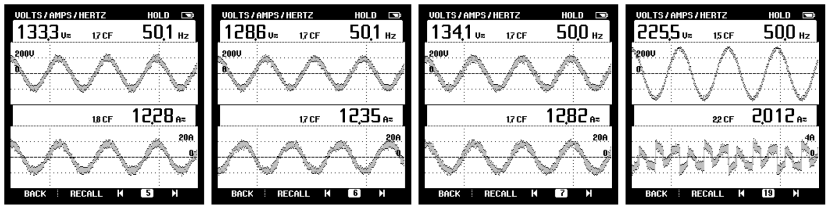


*a* *b* *c* *d*

**Fig. 5** *Steady-state response of PV-ECS at non-linear load*
***(a)–(d)*** Wave shapes of $v_{sa}$, $i_{VSIa}$, $v_{sb}$, $i_{VSIb}$, VSI, $i_{VSIc}$, $v_{sbc}$, $i_{VSIn}$

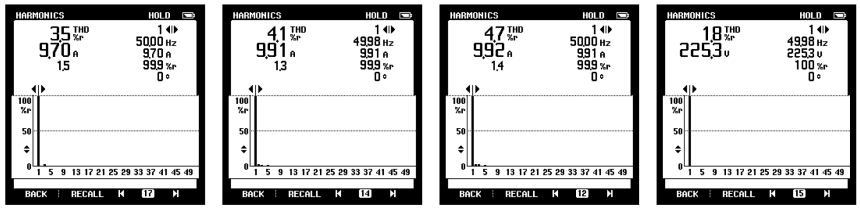


*a* *b* *c* *d*

**Fig. 6** *Steady-state responses of PV-ECS at non-linear load*
***(a)–(d)*** THD spectra of $i_{sa}$, $i_{sb}$, $i_{sc}$, $v_{sbc}$

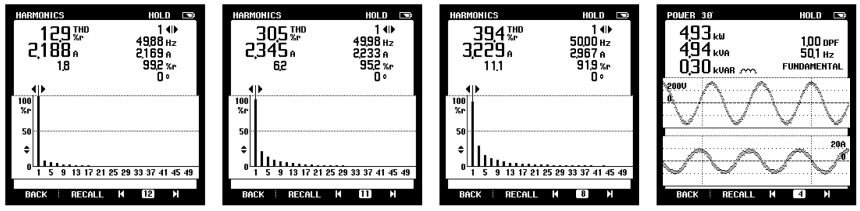


*a* *b* *c* *d*

**Fig. 7** *Steady-state responses of PV-ECS at non-linear load*
***(a)–(c)*** THD spectra of $i_{La}$, $i_{Lb}$, $i_{Lc}$, ***(d)*** Three-phase SPV-VSI power per phase

Figs. 7*d* and 8*a–d* depict the three-phase SPV-VSI power, three-phase grid power ($P_g$) and load power per phase for all the single-phase non-linear loads connected at the PoI. The load neutral current is mitigated by VSI neutral current and neutral current on the grid side is maintained nearly zero.

### *4.2 System behaviour at unbalanced loads*

Figs. 9*a–d* present the dynamic response of control internal signals and system with neutral current compensation when subjected to unbalanced non-linear loads. In Fig. 9*a*, non-linear load connected on the phase '*a*' is disconnected, and then the grid starts absorbing more power from the PV-ECS. The grid current ($i_{sa}$) increased in magnitude slightly as load current component of phase '*a*' is small and is maintained sinusoidal. The $V_{dc}$ is regulated constant at a value produced by MPPT of solar PV array and the system operates at UPF operation.

As shown in Fig. 9*b*, when the load is disconnected, the neutral current flowing on the load side is increased, which is compensated by the VSI neutral current while maintaining neutral current on the

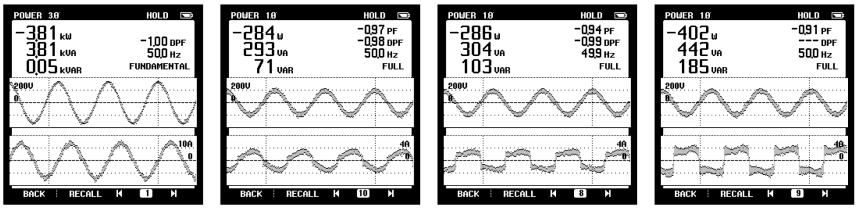


**Fig. 8** *Steady-state responses of PV-ECS at non-linear load*
***(a)*** Three-phase grid power, ***(b)–(d)*** Load powers per phase

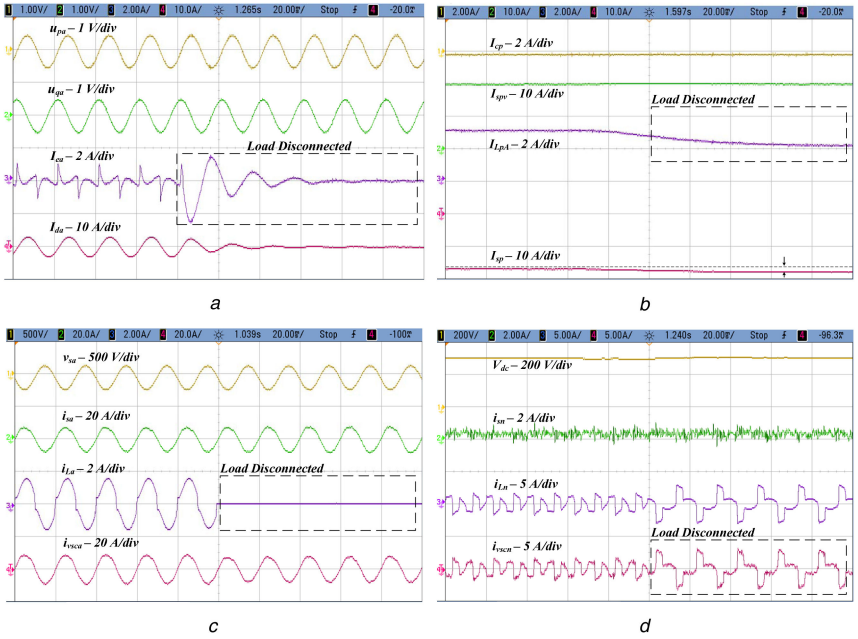


**Fig. 9** *Dynamic performance under unbalanced load*
***(a), (b)*** Response of control internal signals of PV-ECS at unbalanced load, ***(c)*** Dynamic responses of PV-ECS at unbalanced load, ***(d)*** Neutral current compensation

grid side to nearly zero. Figs. 9*c* and *d* show variation in internal signals on the effect of load unbalancing with variations in the error signal ($I_{ea}$) at phase '*a*' filtered component ($I_{da}$) and loss component ($I_{cp}$), PV component ($I_{spv}$), average component ($I_{LpA}$) and reference component ($I_{sp}$).

### *4.3 System behaviour at varying solar irradiance*

The PV-ECS operation is tested under three situations: step change in irradiance level, unavailability of solar power and availability of solar power.

Figs. 10*a* and *b* present the performance of the system when irradiance level of PV array is changed from 600 to 1000 W/m$^2$. The behaviour of control intermediate signals ($I_{dl}$, $I_{ff}$, $I_{Ad}$ and $I_d$), $i_a$, $i_{cnva}$ and $I_{pv}$ is observed. However, the value of $V_{dc}$ is unaffected. Figs. 10*c* and *d* present power-tracking response of PV array, which is maintained at nearly 100% under both irradiance levels. When the irradiance is increased, MPP is shifted to its next MPP thereby extracting maximum power at different irradiance levels.

Fig. 11*a* presents the performance of PV-ECS when the solar irradiance level is zero. Initially, PV-ECS supplies power to the grid and tied load, but when PV array generation is zero, the VSI behaves as SAPF supplying compensation current ($i_{cnva}$) and the grid starts supplying power to the connected load. The grid current ($i_a$) changes its phase by 180° and remains sinusoidal. Moreover, the $V_{dc}$ increases to achieve its steady-state value ($V_{dc} = V_{dc}^* = V_{dc\_DST}$).

Finally, Fig. 11*b* presents dynamic responses of system when the radiation is available, i.e. PV array is generating power. The VSI then behaves as compensating device, supplying and transferring active power to the grid and loads maintaining power quality within allowable limits at PoI. Tests results show that the VSI is used at its full potential in different conditions, which boosts the utilisation factor of the device.

## 5 Conclusion

A dual-function single-stage PV-ECS integrated to the 3P4W distribution grid has been proposed here. Two modes of operation of PV-ECS are to supply and transfer active power to the grid and tied loads as well as to improve quality of power at PoI. An InC-based approach is utilised here for tracking MPP of solar PV array and a 3M-PLL-based control scheme is utilised for extracting fundamental components of load current. Simulated and test results have demonstrated the performance of the system under various conditions such as non-linear loading, unbalanced loading and varying irradiance levels. Test results have shown that the system has improved the power quality at the PoI by compensating neutral current and reactive power, correcting power factor and balancing loads on the grid side. The harmonics are reduced to below 5% on grid side, which is within the limits of an IEEE-519 standard. Moreover, test results have indicated that the system has operated suitably during night-time (sunlight unavailability) thereby increasing the utilisation factor of the VSI by two-fold. The single-stage structure has decreased the losses in the system and increased the total efficacy of the system.

## 6 Acknowledgment

The authors are thankful to the Department of Science and Technology, Govt. of India, for supporting the project under RP02583 grant number.

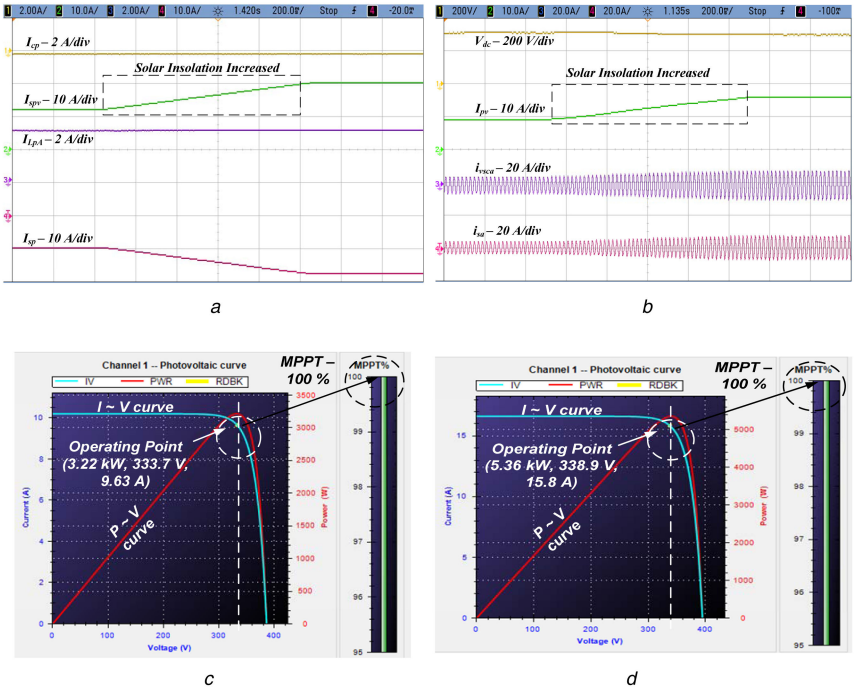


*a* *b* *c* *d*

**Fig. 10** *Dynamic performance under varying insolation*

***(a)*** Response of control internal signals of PV-ECS, ***(b)*** Dynamic performance of PV-ECS with step increase in irradiance from 600 to 1000 W/m$^2$, ***(c), (d)*** MPPT responses of the system at 600 and 1000 W/m$^2$

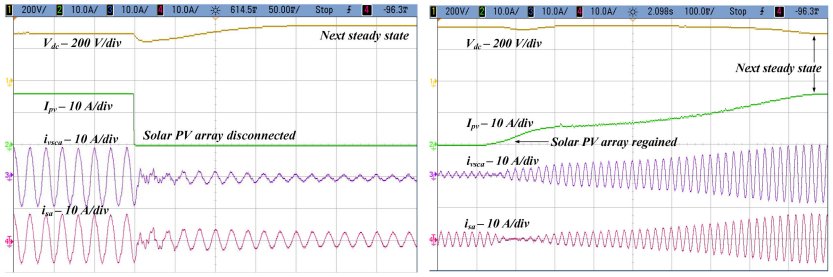


*a* *b*

**Fig. 11** *Dynamic performance under varying modes*

***(a)*** Solar PV array power disconnected, ***(b)*** Solar PV array power regained

## 7 References


[1] Muro, M., Saha, D.: 'Why rooftop solar – and full retail feed in tariffs – benefits all consumers', 30 May 2016. Available at http://reneweconomy.com.au/2016/rooftop-solar-net-metering-is-a-net-benefit-28170

[2] Meza, E.: 'India implements new 40 GW rooftop, small PV plant program', 20 May 2016. Available at http://www.pv-magazine.com/news/details/beitrag/india-implements-new-40-gw-rooftop--small-pv-plant-program-_100024678/#axzz4ADc3MIV6

[3] Deo, S., Jain, C., Singh, B.: 'A PLL-less scheme for single-phase grid interfaced load compensating solar PV generation system', *IEEE Trans. Ind. Inf.*, 2015, **11**, (3), pp. 692–699

[4] Yang, Y., Blaabjerg, F., Wang, H., *et al.*: 'Power control flexibilities for grid-connected multi-functional photovoltaic inverters', *IET Renew. Power Gener.*, 2016, **10**, (4), pp. 504–513

[5] Agarwal, R., Hussain, I., Singh, B.: 'LMF based control algorithm for single stage three-phase grid integrated solar PV system', *IEEE Trans. Sust. Energy*, 2016, **7**, (4), pp. 1379–1387

[6] Singh, B., Chandra, A., Al-Haddad, K.: '*Power quality: problems and mitigation techniques*' (John Wiley & Sons Ltd., U.K, 2015)

[7] Qasim, M., Kanjiya, P., Khadkikar, V.: 'Artificial-neural-network-based phase-locking scheme for active power filters', *IEEE Trans. Ind. Electron.*, 2014, **61**, (8), pp. 3857–3866

[8] Srinivas, M., Hussain, I., Singh, B.: 'Combined LMS-LMF based control algorithm of DSTATCOM for power quality enhancement in distribution system', *IEEE Trans. Ind. Electron.*, 2016, **63**, (7), pp. 4160–4168

[9] Singh, M., Chandra, A.: 'Real-time implementation of ANFIS control for renewable interfacing inverter in 3P4W distribution network', *IEEE Trans. Ind. Electron.*, 2013, **60**, (1), pp. 121–128

[10] Sekhar, V.C., Kant, K., Singh, B.: 'DSTATCOM supported induction generator for improving power quality', *IET Renew. Power Gener.*, 2016, **10**, (4), pp. 495–503

[11] Zou, Z.-X., Zhou, K., Wang, Z., *et al.*: 'Frequency-adaptive fractional-order repetitive control of shunt active power filters', *IEEE Trans. Ind. Electron.*, 2015, **62**, (3), pp. 1659–1668

[12] Panigrahi, R., Subudhi, B., Panda, P.C.: 'A robust LQG servo control strategy of shunt-active power filter for power quality enhancement', *IEEE Trans. Power Electron.*, 2016, **31**, (4), pp. 2860–2869

[13] Espinoza-Trejo, D.R., Bárcenas-Bárcenas, E., Campos-Delgado, D.U., *et al.*: 'Voltage-oriented input–output linearization controller as maximum power point tracking technique for photovoltaic systems', *IEEE Trans. Ind. Electron.*, 2015, **62**, (6), pp. 3499–3507

[14] Paz, F., Ordonez, M.: 'High performance solar MPPT using switching ripple identification based on a lock-in amplifier', *IEEE Trans. Ind. Electron.*, 2016, **63**, (6), pp. 3595–3604

[15] Kish, G.J., Lee, J.J., Lehn, P.W.: 'Modelling and control of photovoltaic panels utilising the incremental conductance method for maximum power point tracking', *IET Renew. Power Gener.*, 2012, **6**, (4), pp. 259–266

[16] Sekhar, P.C., Mishra, S.: 'Takagi–sugeno fuzzy-based incremental conductance algorithm for maximum power point tracking of a photovoltaic generating system', *IET Renew. Power Gener.*, 2014, **8**, (8), pp. 900–914

[17] Soon, T.K., Mekhilef, S.: 'A fast-converging MPPT technique for photovoltaic system under fast-varying solar irradiation and load resistance', *IEEE Trans. Ind. Inf.*, 2015, **11**, (1), pp. 176–186

[18] Mohanty, S., Subudhi, B., Ray, P.K.: 'A new MPPT design using grey wolf optimization technique for photovoltaic system under partial shading conditions', *IEEE Trans. Sustain. Energy*, 2016, **7**, (1), pp. 181–188

[19] Mohd Zainuri, M.A.A., Mohd Radzi, M.A., Soh, A.C., *et al.*: 'Development of adaptive perturb and observe-fuzzy control maximum power point tracking for photovoltaic boost dc-dc converter', *IET Renew. Power Gener.*, 2014, **8**, (2), pp. 183–194

[20] Elobaid, L.M., Abdelsalam, A.K., Zakzouk, E.E.: 'Artificial neural network-based photovoltaic maximum power point tracking techniques: a survey', *IET Renew. Power Gener.*, 2015, **9**, (8), pp. 1043–1063

[21] Chen, S.H., Huang, T.C., Ng, S.S., *et al.*: 'A direct AC–DC and DC–DC cross-source energy harvesting circuit with analog iterating-based MPPT

technique with 72.5% conversion efficiency and 94.6% tracking efficiency', *IEEE Trans. Power Electron.*, 2016, **31**, (8), pp. 5885–5899

[22] Khan, O., Xiao, W., Zeineldin, H.H.: 'Gallium-Nitride-based submodule integrated converters for high-efficiency distributed maximum power point tracking PV applications', *IEEE Trans. Ind. Electron.*, 2016, **63**, (2), pp. 966–975

[23] Killi, M., Samanta, S.: 'An adaptive voltage-sensor-based MPPT for photovoltaic systems with SEPIC converter including steady-state and drift analysis', *IEEE Trans. Ind. Electron.*, 2015, **62**, (12), pp. 7609–7619

[24] Karimi-Ghartemani, M.: 'A novel three-phase magnitude-phase-locked loop system', *IEEE Trans. Circuits Syst. I, Regular Papers*, 2006, **53**, (8), pp. 1792–1802

[25] Hsieh, G.-C., Hung, J.C.: 'Phase locked loop techniques: A survey', *IEEE Trans. Ind. Electron.*, 1996, **43**, (6), pp. 609–615

[26] Villalva, M.G., Gazoli, J.R., Filho, E.R.: 'Comprehensive approach to modeling and simulation of photovoltaic arrays', *IEEE Trans. Power Electron.*, 2009, **24**, (5), pp. 1198–1208

[27] Akagi, H., Watanabe, E.H., Aredes, M.: '*Instantaneous power theory and applications to power conditioning*' (Wiley-IEEE Press, Hoboken, NJ, 2007)

[28] IEEE Recommended Practices and requirement for Harmonic Control on Electric Power System, IEEE Std.519, 1992